

1 **Title:** **Mechanistic insights into heterogeneous**
2 **radiofrequency ablation effects at the left atrial**
3 **posterior wall during pulmonary vein isolation**
4
5 **Author:** David R. Tomlinson BM BSc MD
6 **Corresponding address:** University Hospitals Plymouth NHS Trust, South West
7 Cardiothoracic Centre, Derriford Hospital, Plymouth, UK, PL6
8 8DH
9 **Tel:** 01752 431838
10 **Email:** david.tomlinson1@nhs.net
11 **Word count:** Abstract 250; body text 3663

12
13
14
15
16
17
18
19

20 **Abstract**

21 **Background**

22 Independent investigations demonstrate greater radiofrequency (RF) ablation effects at left-
23 sided left atrial posterior wall (LAPW) sites.

24 **Objective**

25 To investigate mechanisms underlying RF ablation heterogeneity during contact-force (CF)
26 and VISITAG™ Module (Biosense Webster)-guided pulmonary vein isolation (PVI).

27 **Methods**

28 Consecutive patients undergoing PVI during atrial overdrive pacing comprised 2 cohorts:
29 intermittent positive pressure ventilation (IPPV, 14-16/min, 6-8ml/kg); high frequency jet
30 ventilation (HFJV, 150/min, Monsoon III, Acutronic). Temperature-controlled (17ml/min,
31 48°C) RF data was retrospectively assessed at first-annotated (target 15s) LAPW sites: 30W
32 during IPPV; 20W at left-sided sites during HFJV.

33 **Results**

34 Twenty-five and 15 patients underwent PVI during IPPV and HFJV, respectively. During
35 IPPV, left versus right-sided median impedance drop (ImpD) was 13.6Ω versus 9.9Ω
36 ($p<0.0001$) respectively and mean time to pure R unipolar electrogram (UE) morphology
37 change 4.9s versus 6.7s ($p=0.007$) respectively. During HFJV, ImpD was greater at left-sided
38 sites (9.7Ω versus 7.4Ω, $p=0.21$) and time to pure R UE significantly shorter: 4.3s versus 6.1s
39 ($p=0.02$). Minimum case impedance subtracted from pre-RF baseline impedance (BI)
40 generated site-specific Δ BI. Left-sided sites demonstrated significantly greater Δ BI,
41 correlating strongly with $\ln(\text{ImpD})$ – IPPV $r=0.84$ (0.65 – 0.93), HFJV $r=0.77$ (0.35 – 0.93).

42 At right-sided sites, ΔBI and $\text{Ln}(\text{ImpD})$ were without correlation during IPPV, but correlation
43 was modest during HFJV ($r=0.54, -0.007 - 0.84$).

44 **Conclusions**

45 ΔBI may usefully indicate catheter-tissue contact surface area (SA). Consequently, greater
46 left-sided LAPW RF effect may result from greater contact SA and in-phase catheter-tissue
47 motion; HFJV may reduce right-sided out-of-phase catheter-tissue motion. Modifying RF
48 delivery based on ΔBI may improve PVI safety and efficacy.

49

50

51

52

53

54

55

56

57

58

59

60

61

62 **Introduction**

63 Pulmonary vein electrical isolation (PVI) is considered a prerequisite for atrial fibrillation
64 (AF) ablation success.¹ However, delivering permanently overlapping and transmural (TM)
65 lesions without complications is a complex undertaking; on the one hand, non-TM lesions
66 result in late pulmonary vein (PV) electrical gaps and recurrent AF², whereas excessive focal
67 radiofrequency (RF) energy delivery risks life-threatening extra-cardiac thermal trauma.³

68 Recently, RF annotation modules have been developed in an effort to provide guidance
69 towards appropriate “per-site” RF delivery during RF PVI. These include novel systems for
70 assessing the adequacy of “per-site” RF lesions, using weighted formulae incorporating
71 catheter-tissue contact-force (CF), RF power and duration.⁴ Sites of RF application are
72 automatically displayed on a 3-D electroanatomical map using objective descriptors of
73 catheter stability, theoretically facilitating the development of safe, effective and reproducible
74 PVI protocols.⁵ Subsequent studies have demonstrated how, following the derivation of
75 putative ideal “per-site” targets for RF delivery via retrospective analyses of VISITAG™
76 Module annotation (Biosense Webster Inc., Diamond Bar, CA), >90% freedom from
77 implantable loop recorder (ILR)-detected AF may result from active CF and VISITAG™
78 Module guidance during PVI.⁶ However, in this “CLOSE-guided” PVI 85 patient cohort,
79 75% experienced intra-oesophageal temperature rise >38.5°C (ITR, SensiTherm™, Abbott),
80 totalling 183 episodes.⁷ Furthermore, the significantly greater proportion of ITR events
81 occurring at the left-side of the LAPW indicates possible heterogeneity of RF effect at the LA
82 posterior wall (LAPW). Such heterogeneity of RF effect during PVI has been demonstrated
83 previously, with independently conducted investigations providing evidence towards
84 significantly greater RF effect at left-sided left atrial sites.^{8,9} More recently and via
85 retrospective analyses of VISITAG™ Module annotated sites, ~30% greater RF effect was
86 demonstrated at the left side of the LAPW, evidenced by significantly greater absolute

87 impedance decrease and shorter time to pure R unipolar electrogram (UE) morphology
88 change¹⁰ – a histologically validated marker of transmural (TM) RF effect in atrial tissue, *in*
89 *vivo*.^{11,12} Importantly, off-line analyses of exported catheter RF and position data indicated
90 that these findings were neither due to differences in RF duration, nor simply greater catheter
91 instability and/or lower CF at right-sided LAPW sites.¹⁰

92 Taken together, these data indicate significantly greater RF effect at the left side of the
93 LAPW of clinical relevance, yet without mechanistic explanation. One possibility is the
94 occurrence of cardiac and/or respiratory cycle-induced site-specific differences in the
95 magnitude of out-of-phase (i.e. sliding) catheter-tissue interaction. While it is neither
96 desirable nor technically possible to perform PVI during complete atrial and ventricular
97 standstill, high frequency jet ventilation (HFJV) provides means to eliminate respiratory
98 cycle-induced changes in catheter-tissue interaction. Therefore, the aim of this present report
99 was to retrospectively assess the magnitude of RF effects at first-ablated left and right-sided
100 LAPW sites in consecutive cohorts of patients undergoing PVI during either intermittent
101 positive pressure ventilation (IPPV), or HFJV.

102

103 **Methods**

104 Single-operator (DRT) CF and VISITAG™ Module-guided PVI was performed employing a
105 previously reported protocol¹⁰ in consecutive, unselected adult patients with symptomatic AF
106 undergoing first-time PVI according to current treatment indications.¹ All procedures were
107 undertaken using general anaesthesia (GA) with endotracheal intubation. Single transseptal
108 access was obtained with an SL1 (Abbott Cardiovascular, St Paul, MN) sheath, following
109 which either a NaviStar® THERMOCOOL® SMARTTOUCH™ (ST) F curve or NaviStar®
110 EZSTEER® THERMOCOOL® SMARTTOUCH™ D/F catheter (Biosense Webster) via an

111 Agilis™ NxT sheath (Abbott) was placed in the LA via the first transseptal site.
112 ACCURESP™ respiratory training was undertaken pre-ablation and applied as required to
113 the CARTO® geometry, created using a LASSO® Nav catheter (Biosense Webster). Where
114 respiratory motion was insufficient to trigger the ACCURESP™ detection threshold the tidal
115 volume was never deliberately increased, but where ACCURESP™ respiratory adjustment
116 threshold was exceeded, VISITAG™ Module filter preferences during ablation employed
117 ACCURESP™ set “off” to avoid RF annotation error.¹³ The IPPV cohort employed fixed 6-
118 8ml/kg ventilation at 14-16 breaths per minute, guided by end-tidal CO₂; positive end-
119 expiratory pressure 5cmH₂O; 50% inspired oxygen concentration. For the HFJV cohort, GA
120 was induced and maintained with a total intravenous anaesthesia technique guided by depth
121 of anaesthesia monitoring (BIS™, Medtronic Inc., St Paul, MN). IPPV was employed until
122 the mapping and ablation phases of the procedure, whereupon HFJV (Monsoon III, Acutronic
123 Medical Systems AG, Hirzel, CH) was used via a jet ventilation catheter; inspired oxygen
124 concentration 60% (titrated to maintain oxygen saturations $\geq 95\%$); ventilation frequency 150
125 jets/min; driving pressure 1.0 bar with 1:1 inspiration to expiration ratio.

126 A SkinTact® RO01B30 indifferent electrode (Leonhard Lang GmbH, Innsbruck, AT) was
127 placed on the shaved skin of the thigh posterolaterally, contralateral to any orthopaedic
128 prostheses. VISITAG™ Module and CF-guided PVI was performed during proximal pole CS
129 pacing at 600ms using temperature-controlled RF (48°C, 17ml/min irrigation) via an EP
130 Shuttle® (Stockert GmbH, Freiburg, DE) generator and ThermoCool® SmartTouch® catheter
131 using Agilis™ NxT sheath (Abbott) support. VISITAG™ Module filter preferences for
132 automated RF annotation were: Positional stability range 2mm, tag display duration 3s; force-
133 over-time 100% minimum 1g (the latter to ensure on-going RF annotation only in the
134 presence of constant catheter-tissue contact¹⁴). Lesion placement was guided by VISITAG™
135 Module annotation, with the preferred site of first RF application at the LAPW opposite each

136 superior PV ~1cm from the PV ostium; in cases where constant catheter-tissue contact could
137 only be achieved with maximal CF $\geq 70g$, an adjacent LAPW site with lower peak CF was
138 chosen. The target annotated RF duration at each first-ablated LAPW site was 15s, whereas
139 ~9-11s was the target for consecutive, adjacent sites during continuous RF delivery. Target
140 inter-tag distance (ITD) $\leq 6mm$ was achieved using rapid movement of the catheter tip
141 initiated via the Agilis sheath, aided by the distance measurement tool; point-by-point (PbP)
142 RF was also applied as necessary to achieve this end-point.

143 For the IPPV cohort, 30W RF was used at all sites. However, in view of previous
144 investigations demonstrating ~30% greater RF effect at the left-side of the LAPW¹⁰, 20W
145 was the peak power used during first encirclement at left-sided LAPW sites during HFJV. In
146 addition to the RF duration targets described, annotated “per site” LAPW targets during
147 HFJV included a minimum impedance drop of 3Ω . Following completion of circumferential
148 PVI (entrance and exit block), spontaneous recovery of PV conduction was assessed and
149 eliminated during a minimum 20-minute wait; dormant recovery was evaluated and
150 eliminated a minimum of 20 minutes after the last RF. Neither oesophageal luminal
151 temperature monitoring nor post-ablation endoscopic evaluation was employed.

152 This work received IRB approval for publication as a retrospective service evaluation. All
153 patients provided written, informed consent.

154 **Analyses**

155 Annotated first-site RF duration, mean CF and impedance drop (ImpD) data were obtained
156 via the proprietary VISITAG™ Module export function. Bipolar electrogram (BE) peak-to-
157 peak amplitude and the timing of unipolar electrogram (UE) morphology change from RS to
158 pure R data were retrospectively obtained from CARTOREPLAY™ (Biosense Webster) as
159 previously described.¹⁰ Exported text files were converted to Excel data and imported to

160 GraphPad Prism version 4.03 (GraphPad Software, San Diego, CA). For correlation analyses,
161 ImpD data was Ln transformed to achieve a normal distribution. Considering the known
162 importance of the surface area (SA) of catheter-tissue contact towards RF lesion creation¹⁵, a
163 hypothetical indicator of the ablation catheter-tissue SA at RF onset was retrospectively
164 derived from VISITAG™ Module-based ablation catheter (unipolar) impedance data. This
165 was calculated by subtracting the minimum case impedance value (from the exported
166 “AblationData” file) from the immediate pre-RF onset impedance (i.e. “Base impedance”,
167 BI), to derive the site-specific delta base impedance (Δ BI).

168 **Statistics**

169 Comparisons were made based on the means and standard deviations [SD] of biophysical
170 data (i.e. ILD, RF duration, CF, ImpD), or medians along with the 1st and 3rd quartile (IQR),
171 where these data were determined to be skewed. Differences in the biophysical data between
172 IPPV and HFJV, and left and right-sided LAPW sites were tested using the unpaired t-test, or
173 the Mann-Whitney test where data could not be assumed to be normally distributed. The
174 Pearson or Spearman correlation coefficient was calculated to determine the strength of
175 association between Ln (ImpD) and both BI and Δ BI, as appropriate. In this exploratory
176 analysis, significance was set at the 5% level.

177

178 **Results**

179 The IPPV cohort comprised 25 patients (November 2016 – May 2017): 13 persistent AF, 12
180 PAF; 19 male (76%); mean age 57 [14] years and CHA₂DS₂-VASc score 1.3 [1.3]. The
181 HFJV cohort comprised 15 patients (July 2018 – June 2019): 9 persistent AF, 6 PAF; 12 male
182 (80%); mean age 60 [9] years and CHA₂DS₂-VASc score 1.2 [1.1]. Complete PVI with the
183 elimination of spontaneous and/or dormant recovery of PV conduction was achieved

184 following 16.2 [3.1] and 20.0 [4.6] minutes of RF for IPPV and HFJV cohorts, respectively.
185 For the IPPV cohort, pulmonary vein (PV) carina RF was applied in 18/25 patients (72%);
186 i.e. left PV carina in 8/25 (32%) and right PV carina in 16/25 (64%). For the HFJV cohort,
187 PV carina RF was applied in 13/15 patients (87%); i.e. left PV carina in 10/15 (67%), right
188 PV carina only 10/15 (67%). There were no procedural complications.

189 In the IPPV cohort, 3 first-ablated sites were excluded from analysis; inadvertent catheter
190 displacement at two left-sided sites resulted in RF annotation termination at 4.4s and 7.9s,
191 while catheter displacement at RF onset resulted in 5.0s non-annotated RF delivery for one
192 right-sided site. In the HFJV cohort, 4 first-ablated sites were excluded from analysis: For
193 one left-sided site, DC cardioversion (DCCV)-refractory AF was present, while inadvertent
194 catheter displacement resulted in RF annotation termination at 7.1s in another; pure R UE
195 morphology change was not achieved at one left-sided site with pre-ablation bipolar
196 electrogram (BE) amplitude 0.7mV, annotated RF duration 14.7s, mean CF 21g, and ImpD
197 8.6Ω - excepting the one case of DCCV-refractory AF, this was the lowest pre-ablation BE
198 amplitude in the HFJV cohort and was considered an outlier; inadvertent catheter
199 displacement resulted in RF annotation termination at 7.6s for one right-sided site.

200 **Biophysical data: IPPV cohort**

201 First-ablated LAPW site biophysical data according to ventilatory protocol and PV pair
202 proximity at the LAPW are shown in table 1. During IPPV and using 30W, annotated RF
203 duration was in keeping with the protocol; i.e. median 14.9s versus 15.0s, left PV (LPV)
204 versus right PV (RPV) aspects of the LAPW respectively. There was no significant difference
205 in pre-ablation BE amplitude; median 1.5mV versus 1.7mV ($p=0.95$), LPV and RPV
206 respectively. Mean CF was significantly greater at RPV LAPW sites; i.e. 16.5g versus 11.2g
207 ($p=0.003$), RPV and LPV respectively. During IPPV, both ImpD and time to pure R UE

208 morphology change data indicated significantly greater RF effects at the left side of the
209 LAPW: median ImpD 13.6Ω versus 9.9Ω ($p<0.0001$), LPV versus RPV respectively; mean
210 time to pure R UE morphology change $4.9s$ versus $6.7s$ ($p=0.007$), LPV versus RPV
211 respectively.

212 During IPPV the mean BI was significantly greater at left-sided LAPW sites; i.e. median
213 182Ω versus 175Ω ($p=0.002$), LPV versus RPV. The mean minimum (total case) impedance
214 was 141Ω , therefore the mean ΔBI was significantly greater at LPV versus RPV sites; i.e.
215 45.0Ω versus 35.3Ω ($p=0.01$), LPV versus RPV respectively. For left-sided LAPW sites, both
216 BI and ΔBI demonstrated significant positive correlation with $\ln(\text{ImpD})$, but correlation was
217 strongest for ΔBI : i.e. BI with $\ln(\text{ImpD})$ Pearson $r=0.66$ ($0.34 - 0.84$, $p=0.0006$); ΔBI with
218 $\ln(\text{ImpD})$ $r=0.84$ ($0.65 - 0.93$, $p<0.0001$). For right-sided LAPW sites, neither BI nor ΔBI
219 demonstrated significant correlation with $\ln(\text{ImpD})$; i.e. Spearman $r=0.33$ ($-0.10 - 0.65$,
220 $p=0.12$) and $r=0.26$ ($-0.18 - 0.61$, $p=0.23$) for BI with $\ln(\text{ImpD})$, and ΔBI with $\ln(\text{ImpD})$
221 respectively (figure 1).

222 **Biophysical data: HFJV cohort**

223 During HFJV, and using 20W and 30W at left and right-sided LAPW sites respectively,
224 annotated RF duration was in keeping with the protocol; i.e. median $14.5s$, both PVs. There
225 was no significant difference in pre-ablation BE amplitude; median $1.5mV$ versus $1.7mV$
226 ($p=0.94$), LPV and RPV respectively. There was no difference in mean CF during HFJV; i.e.
227 $12.5g$ and $12.0g$ ($p=0.61$), LPV versus RPV respectively. During HFJV, median ImpD was
228 greater at LPV sites (9.7Ω versus 7.4Ω , $p=0.21$) but this did not reach statistical significance.
229 However, time to pure R UE morphology change was significantly shorter at LPV sites; i.e.
230 mean $4.3s$ versus $6.1s$ ($p=0.02$), LPV versus RPV respectively.

231 During HFJV the mean BI was significantly greater at left-sided LAPW sites; i.e. 183Ω
232 versus 174Ω (p=0.03), LPV versus RPV respectively. The mean minimum (total case)
233 impedance was 143Ω and 136Ω, LPV and RPV respectively (p=0.25). Therefore, the mean
234 ΔBI was significantly greater at LPV versus RPV sites; i.e. 45.7Ω versus 32.4Ω (p=0.004),
235 LPV versus RPV respectively. At left-sided LAPW sites during HFJV both BI and ΔBI
236 demonstrated significant positive correlation with Ln(ImpD), but correlation was strongest
237 for ΔBI; BI with Ln(ImpD), Pearson r=0.59 (0.03 – 0.87, p=0.04), whereas ΔBI with Ln
238 (ImpD), r=0.77 (0.35 – 0.93, p=0.004). At right-sided LAPW sites during HFJV there was no
239 significant correlation between BI and Ln(ImpD); Spearman r=0.33 (-0.26 – 0.74, p=0.25).
240 However, right-sided LAPW sites during HFJV demonstrated moderate positive correlation
241 for ΔBI with Ln(ImpD); Spearman r=0.54 (-0.007 – 0.84, p=0.047, figure 2).

242 There was no significant correlation between mean CF and Ln(ImpD) within any ventilatory
243 group; i.e. r=-0.24, 0.07, 0.02 and -0.10 for LPV IPPV, RPV IPPV, LPV HFJV and RPV
244 HFJV, respectively.

245

246 **Discussion**

247 The main finding of this present report is that heterogeneity of RF effect at the LAPW was
248 not eliminated using a HFJV protocol; i.e. greater effect remained evident at left-sided sites,
249 despite reducing left-sided LAPW power delivery by 30%. Therefore, although heterogeneity
250 of RF effect cannot be completely explained on the basis of respiratory motion-induced
251 differences catheter-tissue interaction, these present data can be used to derive hypotheses
252 towards other possible mechanisms underlying heterogeneity of RF effects during PVI.

253

254 **Hypothetical mechanisms underlying heterogeneity of RF effects *in vivo***

255 In this present experimental set-up, identical and objectively annotated parameters for
256 position and CF stability – the two presently measurable components of catheter “stability”
257 – were prospectively employed in order to meet a suitable definition of a “stable” point: (1)
258 Position stability range 2mm with ACCURESP “off” – VISITAG™ Module logic previously
259 shown to satisfy “stable point” criteria¹³, and; (2) force-over-time 100%, minimum 1g CF –
260 self-evidently, constant catheter-tissue contact is a prerequisite at “stable” sites.¹⁴ Previous
261 investigations have demonstrated that greater RF effect at left-sided LAPW sites was not
262 simply due to measurably superior position stability.¹⁰ Therefore, assuming equal RF
263 generator power delivery, greater RF effect in this *in vivo* model must result from either
264 greater catheter-tissue interaction stability as a result of significantly lower *out-of-phase* (i.e.
265 sliding) catheter-tissue interaction, and/or a greater SA of catheter-tissue contact.

266 From a theoretical standpoint, if an ablation catheter is kept “positionally stable” and
267 (knowingly) remains stable throughout “per-site” RF delivery without significant out-of-
268 phase catheter-tissue interaction, differences in the SA of catheter-tissue contact will be the
269 principal determinant of measurable differences of RF effects, since:

270
$$\text{“Tissue power” (P)} = I^2 \cdot R$$

271 (I is current density and R, tissue resistance).¹⁵

272 In this theoretical model of stable catheter-tissue interaction, any suitable measure of the SA
273 of catheter-tissue contact will demonstrate strong positive correlation with RF effects.

274 Therefore, this present report’s finding of a strong positive correlation between ΔBI and
275 $\ln(\text{ImpD})$ at left-sided LAPW sites indicates not only that ΔBI may represent a suitable
276 indicator of the SA of catheter-tissue contact *in vivo*, but also that catheter-tissue interaction
277 at left-sided LAPW sites is predominantly *in-phase*. At the right-sided LAPW sites, the

278 significantly lower ΔBI supports the proposition that ΔBI provides a suitable measure of
279 catheter-tissue contact SA. However, during IPPV and despite ablation catheter motion
280 remaining within identical pre-defined limits, the lack of significant correlation between ΔBI
281 and $\text{Ln}(\text{ImpD})$ indicates significant and presently un-measurable, *out-of-phase* catheter-
282 tissue interaction. In contrast, the finding of a modest positive correlation between ΔBI and
283 $\text{Ln}(\text{ImpD})$ at right-sided LAPW sites during HFJV indicates that the operative environment
284 during HFJV is characterised by a reduction in out-of-phase catheter-tissue interaction, but
285 not to the same level of in-phase stability as that inferred using these methods at left-sided
286 LAPW sites.

287 Possible mechanisms for significant differences in the SA of catheter-tissue contact
288 comparing left and right-sided sites could include either/or both of: (1) Differences in the
289 angle of the catheter tip with respect to the target tissue, such that at some sites the contact
290 surface may include both the (tip) face and lateral aspects of the catheter tip, whereas at
291 others, contact is limited to the surface of the (tip) face only; (2) Differences in tissue
292 compliance, with greater SA resulting from more compliant tissue enveloping the catheter tip,
293 potentially even at lower CF. These present data do not permit further conclusions to be
294 drawn regarding the relative importance of these possible mechanisms *in vivo*, however,
295 greater impedance drop has been demonstrated during PVI with parallel or oblique catheter-
296 tissue angle ($30^\circ - 145^\circ$) compared to perpendicular ($0 - 30^\circ$).⁸

297 **Pre-ablation impedance as a possible determinant of RF effect *in vivo***

298 Previous investigations during slow pathway and accessory pathway RF ablation
299 demonstrated strong positive correlation between the initial generator impedance (GI) and
300 electrode temperature during RF delivery.¹⁶ In a pig thigh model of RF ablation using a linear
301 multi-electrode catheter, greater baseline (unipolar) impedance was demonstrated with

302 greater applied downward force, and there was a strong positive correlation between baseline
303 impedance and lesion depth and width.¹⁷ More recently and using an ablation catheter with
304 mini-electrodes incorporated in the distal electrode (Rhythmia™ and IntellaNav MiFi™ OI,
305 Boston Scientific, Marlborough, MA), the predictive utility of baseline generator and local
306 impedances (LI – taken as the maximal value from all three mini electrodes) were
307 investigated during PVI. The baseline GI demonstrated weak positive correlation with
308 subsequent RF-induced GI drop (adjusted $R^2=0.06$, $p<0.001$). However, higher baseline LI
309 predicted higher LI drop during ablation (adjusted $R^2=0.41$, $p<0.001$).¹⁸ Lastly, finite element
310 modelling of a 7F 4mm ablation catheter and homogeneous tissue slab (4mm thickness) with
311 simulations of varying depth and angle of catheter-tissue interaction, demonstrated a very
312 strong positive correlation between increasing contact area and impedance ($R=0.97$).
313 Moreover, while the impedance increased at greater depth of catheter-tissue penetration, the
314 catheter angle was a significant determinant of impedance; incrementally greater impedance
315 was noted as the angle was decreased from 90° to 15° in 15° steps. Importantly, catheter angle
316 was a more important determinant of impedance at greater modelled depth of tissue
317 penetration.¹⁹

318 **Clinical implications**

319 The inference of both significantly greater *in-phase* catheter-tissue interaction and greater SA
320 of stable contact at left-sided LAPW sites provides the perfect milieu for inadvertent extra-
321 cardiac thermal trauma from a “one-size-fits-all”, single RF power and duration delivery
322 protocol during PVI. Similarly, ablation protocols employing identical LAPW RF targets
323 using theoretical composite measures of RF delivery (i.e. Ablation Index – AI, or VISITAG
324 SURPOINT™, Biosense Webster – and lesion size index – LSI, Abbott) will also result in
325 heterogeneous tissue injury during PVI, perpetuating this risk.^{4,6} This is particularly
326 concerning in view of the more frequently occurring left-sided oesophageal position²⁰ and

327 high case fatality rates of ablation-induced atrio-oesophageal fistula.²¹ Therefore for greater
328 safety, operators may wish to consider adopting protocols involving lower RF power, shorter
329 RF duration and/or lower AI/LSI targets at the left side of the LAPW, or simply utilising
330 more direct and *in vivo* validated measures of tissue RF effect including impedance drop
331 and/or pure R UE morphology change.^{10,22–24}

332 Since Δ BI may represent a useful site-specific *pre-ablation predictor* of RF effect, operators
333 may wish to mimic this described operative “stability set-up”. Specifically, with Δ BI
334 representing a putative predictor of RF effect within this reproducible “operative stability
335 environment”, the risk of extra-cardiac thermal trauma during RF delivery using higher
336 power (50-90W) over very short ablation intervals (e.g. 3-5s)^{25,26} – i.e. within potentially very
337 narrow therapeutic windows and involving significant latency²⁷ – may be reduced by
338 modified protocols incorporating Δ BI data. In contrast, protocols using deep conscious
339 sedation with consequent greater random variability of respiratory profile and occasional
340 inadvertent patient movement are unlikely to demonstrate similar predictive utility of Δ BI
341 towards subsequent “per-site” RF effects.

342 **Limitations**

343 Time to pure R UE morphology change is an imperfect indicator of RF effect in the absence
344 of left atrial wall thickness data; i.e. shorter time to pure R alone does not necessarily indicate
345 greater RF effect. The methodology for defining the site-specific ablation catheter-to-tissue
346 contact SA described in this present report (i.e. Δ BI) is theoretical. Indeed, more appropriate
347 methodology towards deriving putative “predictive” Δ BI values would be to subtract the pre-
348 ablation “blood-pool” impedance from site-specific BI. However, at the outset of these
349 present investigations “blood-pool” impedance data were not known to be of potential use,
350 and there were no means to obtain these data retrospectively. Clearly, the hypothesis that pre-

351 ablation Δ BI represents a site-specific predictor of RF effect during PVI requires further
352 investigations using “blood-pool” impedance values.

353 These data are limited by their single operator status, applicability to the operative stability
354 conditions described and choice of RF annotation logic using the VISITAG™ Module.

355 However, such stringent catheter stability criteria alongside measureable (and visible to any
356 operator) VISITAG™ Module data outputs may permit these present investigations to form
357 the basis of knowingly reproducible RF delivery *in vivo*, both on an intra and inter-operator
358 basis. These data should not be considered applicable to TactiCath™-based ablation (Abbott),
359 since according to the dimensions of the ablation catheter tip electrode, angle-dependent
360 changes in the SA of contact will result in catheter-specific differences in tissue RF current
361 density and ablation effect.²⁸

362 RF power output from the EP Shuttle® RF generator has been shown to vary according to the
363 pre-ablation impedance; i.e. comparing 30W at 150Ω versus 200Ω, power output at 200Ω
364 was 14% greater, measuring 34.1W.²⁹ However, differences between left and right-sided
365 LAPW BI values in this present report (IQR 177 – 196 and 170 – 180 for LPV and RPV,
366 respectively) were probably insufficient to importantly influence generator RF power output
367 and furthermore, greater RF effect remained at left-sided sites during HFJV despite 30%
368 lower power delivery at left-sided sites.

369

370 **Conclusions**

371 These data support the hypothesis that greater RF ablation effect at left-sided LAPW sites
372 results from significantly greater SA of catheter-to-tissue contact and in-phase catheter-tissue
373 motion. However, HFJV may usefully reduce out-of-phase catheter-tissue motion at right-

374 sided LAPW sites. Using suitably stable and reproducible conditions of catheter-tissue
375 contact, Δ BI may represent a useful site-specific predictor of RF ablation effect, towards
376 improving the safety and efficacy of PVI.

377

378 **Acknowledgements**

379 I am grateful to Cherith Wood, Daniel Newcomb and Ian Lines, Cardiac Physiologists, for
380 their technical support into all cases conducted during this report and Dr David Adams and
381 Dr Kate Holmes for establishing and delivering the HFJV protocol. I am also grateful to
382 Robert Pearce and Vicky Healey (Biosense Webster Inc.) for additional technical assistance
383 and to Noam Seker-Gafni, Tal Bar-on, Einav Geffen, Assaf Rubissa and colleagues at the
384 Haifa Technology Center, Israel for their help with VISITAG™ Module technical queries. I
385 am grateful to Katie Biscombe, John True, Joanne Hosking and Adam Streeter (Department
386 of Medical Statistics, Plymouth University Peninsula Schools of Medicine and Dentistry) for
387 their previous R code development and analyses permitting reference to previously identified
388 measures of catheter stability in this present report.

389

390 **Sources of Funding**

391 Nil

392

393 **Disclosures**

394 None

395

396 **Table legends**

397 Table 1: Biophysical data according to ventilatory protocol and pulmonary vein (PV) pair
398 proximity (i.e. left and right PV, LPV and RPV, respectively) at first-ablated LAPW sites.
399 Data shown are mean [SD] and median (1st – 3rd quartile), as appropriate (BE,
400 CARTOREPLAY™-derived peak-to-peak bipolar electrogram amplitude; BI, baseline
401 impedance; Δ BI, minimum case impedance subtracted from BI; Ln(ImpD), natural log of the
402 annotated impedance drop).

403

404

405

406

407

408

409

410

411

412

413

414

415

| | IPPV (N=25) | | | HFJV (N=15) | | |
|--|-----------------------|------------------------|---------|-----------------------|-------------------------|-------|
| | LPV (30W; N=23) | RPV (30W; N=24) | p | LPV (20W; N=12) | RPV (30W; N=14) | p |
| RF duration (s) | 14.9 (14.3 – 15.7) | 15.0 (14.6 – 15.4) | 0.70 | 14.5 (14.1 – 15.1) | 14.5 (13.7 – 15.0) | 0.40 |
| Pre-RF BE (mV) | 1.5 (1.1 – 3.1) | 1.7 (1.0 – 2.3) | 0.95 | 1.5 (1.1 – 2.9) | 1.7 (1.0 – 3.1) | 0.94 |
| Mean CF (g) | 11.2 (9.0 – 13.4) | 16.5 (12.2 – 18.4) | 0.003 | 12.5 (10.0 – 14.9) | 12.0 (9.4 – 12.2) | 0.61 |
| Impedance drop (Ω) | 13.6 (12.2 – 24.4) | 9.9 (7.9 – 11.6) | <0.0001 | 9.7 (7.2 – 13.7) | 7.4 (6.7 – 9.6) | 0.21 |
| Time to pure R UE (s) | 4.9 [2.1] | 6.7 [2.5] | 0.007 | 4.3 [1.4] | 6.1 [2.1] | 0.02 |
| BI (Ω) | 182 (177 – 196) | 175 (170 – 180) | 0.002 | 183 (175 – 201) | 174 (160 – 182) | 0.03 |
| Δ BI (Ω) | 45.0 [15.2] | 35.3 [9.0] | 0.01 | 45.7 [9.4] | 32.4 [9.0] | 0.004 |
| Pearson/Spearman r: BI vs Ln (ImpD) | 0.66 (0.34 – 0.84) | 0.33 (-0.10 – 0.65) | NA | 0.59 (0.03 – 0.87) | 0.33 (-0.26 – 0.74) | NA |
| Pearson/Spearman r: Δ BI vs Ln (ImpD) | 0.84 (0.65 – 0.93) | 0.26 (-0.18 – 0.61) | NA | 0.77 (0.35 – 0.93) | 0.54 (-0.007 – 0.84) | NA |

Table 1

416 **Figure legends**

417 Figure 1: Correlation between Δ BI and Ln(ImpD) during IPPV according to PV proximity

418 (Pearson / Spearman correlation is displayed, as appropriate).

419

420 Figure 2: Correlation between Δ BI and Ln(ImpD) during HFJV according to PV proximity

421 (Pearson / Spearman correlation is displayed, as appropriate).

422

423

424

425

426

427

428

429

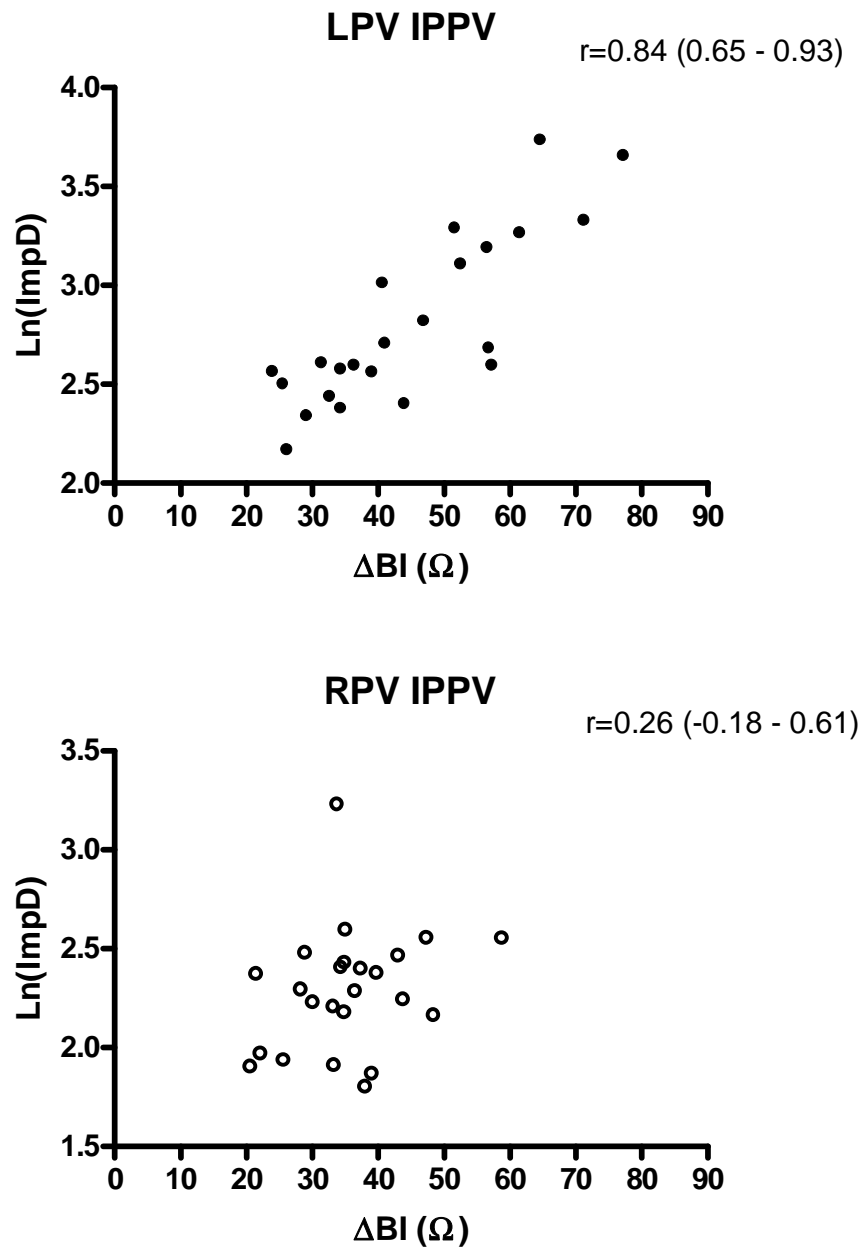
430

431

432

433

434

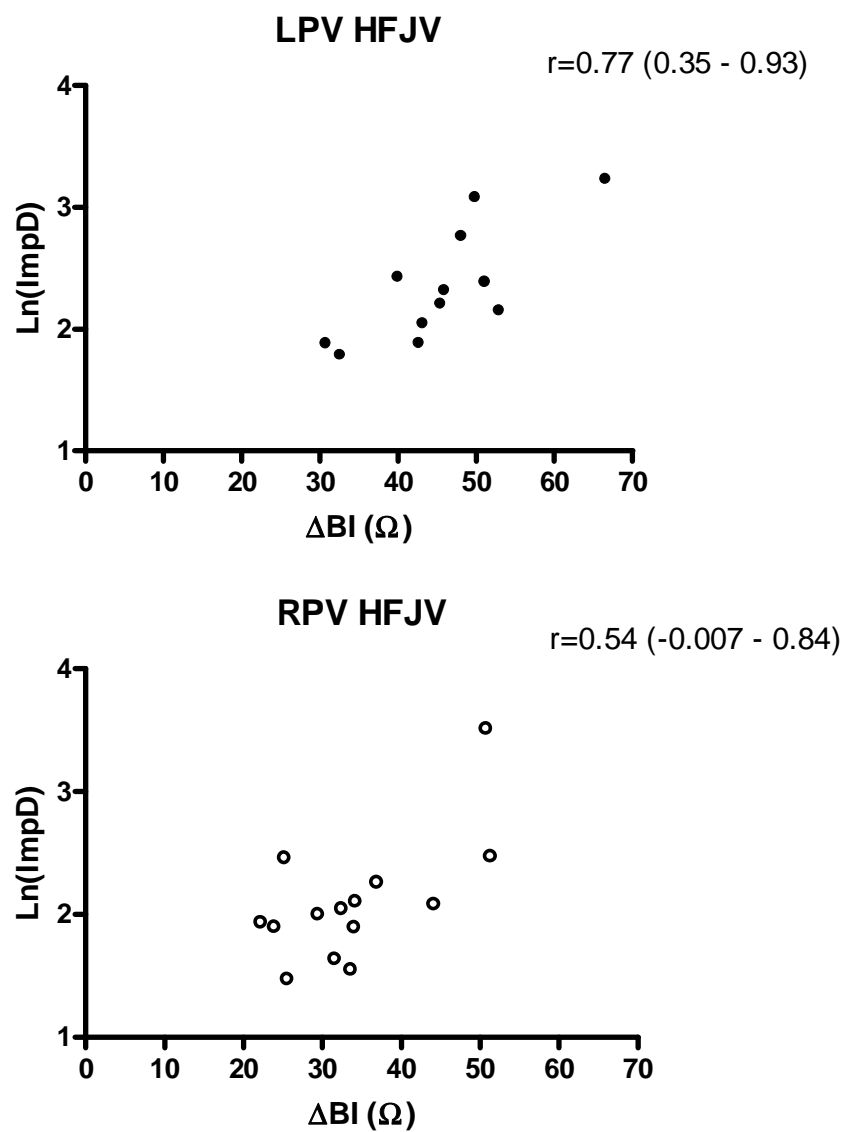


435

436 Figure 1

437

438



439

440 Figure 2

441

442

443

444

445 **References**

- 446 1. Calkins H, Hindricks G, Cappato R, Kim Y-H, Saad EB, Aguinaga L, et al. 2017
447 HRS/EHRA/ECAS/APHRs/SOLAECE expert consensus statement on catheter and
448 surgical ablation of atrial fibrillation. Heart Rhythm [Internet]. 2017 Oct [cited 2019
449 Jan 23];14(10):e275–444. Available from:
450 <http://www.ncbi.nlm.nih.gov/pubmed/28506916>
- 451 2. Kowalski M, Grimes MM, Perez FJ, Kenigsberg DN, Koneru J, Kasirajan V, et al.
452 Histopathologic characterization of chronic radiofrequency ablation lesions for
453 pulmonary vein isolation. J Am Coll Cardiol [Internet]. 2012 Mar 6 [cited 2019 Oct
454 4];59(10):930–8. Available from:
455 <https://linkinghub.elsevier.com/retrieve/pii/S0735109711052697>
- 456 3. Medeiros De Vasconcelos JT, Filho S dos SG, Atié J, Maciel W, De Souza OF, Saad
457 EB, et al. Atrial-oesophageal fistula following percutaneous radiofrequency catheter
458 ablation of atrial fibrillation: the risk still persists. Europace [Internet]. 2016 Oct 6
459 [cited 2017 Nov 20];19(2):euw284. Available from:
460 <http://www.ncbi.nlm.nih.gov/pubmed/28175286>
- 461 4. Das M, Loveday JJ, Wynn GJ, Gomes S, Saeed Y, Bonnett LJ, et al. Ablation index, a
462 novel marker of ablation lesion quality: prediction of pulmonary vein reconnection at
463 repeat electrophysiology study and regional differences in target values. Europace
464 [Internet]. 2016 May 31 [cited 2017 Nov 20];19(5):euw105. Available from:
465 <http://www.ncbi.nlm.nih.gov/pubmed/27247002>
- 466 5. Hussein A, Das M, Riva S, Morgan M, Ronayne C, Sahni A, et al. Use of Ablation
467 Index-Guided Ablation Results in High Rates of Durable Pulmonary Vein Isolation

- 468 and Freedom From Arrhythmia in Persistent Atrial Fibrillation Patients. *Circ*
469 *Arrhythmia Electrophysiol* [Internet]. 2018 Sep [cited 2019 Jan 23];11(9):e006576.
470 Available from: <http://www.ncbi.nlm.nih.gov/pubmed/30354288>
- 471 6. Taghji P, El Haddad M, Philips T, Wolf M, Knecht S, Vandekerckhove Y, et al.
472 Evaluation of a Strategy Aiming to Enclose the Pulmonary Veins With Contiguous and
473 Optimized Radiofrequency Lesions in Paroxysmal Atrial Fibrillation: A Pilot Study.
474 *JACC Clin Electrophysiol*. 2018;4(1):99–108.
- 475 7. Wolf M, El Haddad M, De Wilde V, Philips T, De Pooter J, Almorad A, et al.
476 Endoscopic evaluation of the esophagus after catheter ablation of atrial fibrillation
477 using contiguous and optimized radiofrequency applications. *Hear Rhythm* [Internet].
478 2019 Jul [cited 2019 Oct 4];16(7):1013–20. Available from:
479 <http://www.ncbi.nlm.nih.gov/pubmed/30710736>
- 480 8. Knecht S, Reichlin T, Pavlovic N, Schaer B, Osswald S, Sticherling C, et al. Contact
481 force and impedance decrease during ablation depends on catheter location and
482 orientation: insights from pulmonary vein isolation using a contact force-sensing
483 catheter. *J Interv Card Electrophysiol* [Internet]. 2015 Sep 30 [cited 2019 Jan
484 23];43(3):297–306. Available from: <http://www.ncbi.nlm.nih.gov/pubmed/25925494>
- 485 9. Chelu MG, Morris AK, Kholmovski EG, King JB, Kaur G, Silver MA, et al. Durable
486 lesion formation while avoiding esophageal injury during ablation of atrial fibrillation:
487 Lessons learned from late gadolinium MR imaging. *J Cardiovasc Electrophysiol*
488 [Internet]. 2018 Mar [cited 2019 Jan 23];29(3):385–92. Available from:
489 <http://www.ncbi.nlm.nih.gov/pubmed/29345381>
- 490 10. Tomlinson DR, Myles M, Stevens KN, Streeter AJ. Transmural unipolar electrogram

- 491 change occurs within 7s at the left atrial posterior wall during pulmonary vein
492 isolation. *Pacing Clin Electrophysiol* [Internet]. 2019 May 24 [cited 2019 Jun
493 12];pace.13729. Available from:
494 <https://onlinelibrary.wiley.com/doi/abs/10.1111/pace.13729>
- 495 11. Otomo K, Uno K, Fujiwara H, Isobe M IY. Local unipolar and bipolar electrogram
496 criteria for evaluating the transmural of atrial ablation lesions at different catheter
497 orientations relative to the endocardial surface. *Heart Rhythm*. 2010;7(9):1291–300.
- 498 12. Bortone A, Brault-Noble G, Appetiti A, Marijon E. Elimination of the negative
499 component of the unipolar atrial electrogram as an in vivo marker of transmural lesion
500 creation: acute study in canines. *Circ Arrhythm Electrophysiol* [Internet]. 2015 Aug
501 [cited 2015 Nov 23];8(4):905–11. Available from:
502 <http://www.ncbi.nlm.nih.gov/pubmed/26092576>
- 503 13. Tomlinson DR, Biscombe K, True J, Hosking J, Streeter AJ. Ablation catheter motion
504 detection during contact force and VISITAGTM Module-guided pulmonary vein
505 isolation. *bioRxiv* [Internet]. 2019 Jan 1;631374. Available from:
506 <http://biorxiv.org/content/early/2019/05/08/631374.abstract>
- 507 14. Tomlinson DR. Derivation and validation of a VISITAGTM-guided contact force
508 ablation protocol for pulmonary vein isolation. *bioRxiv* [Internet]. 2017 Dec 13 [cited
509 2017 Dec 14];232694. Available from:
510 <https://www.biorxiv.org/content/early/2017/12/13/232694>
- 511 15. Wittkamp FHM, Nakagawa H. RF Catheter Ablation: Lessons on Lesions. *Pacing*
512 *Clin Electrophysiol* [Internet]. 2006 Nov [cited 2017 Nov 20];29(11):1285–97.
513 Available from: <http://www.ncbi.nlm.nih.gov/pubmed/17100685>

- 514 16. Nsah E, Berger R, Rosenthal L, Hui R, Ramza B, Jumrussirikul P, et al. Relation
515 between impedance and electrode temperature during radiofrequency catheter ablation
516 of accessory pathways and atrioventricular nodal reentrant tachycardia. *Am Heart J*
517 [Internet]. 1998 Nov [cited 2019 Oct 4];136(5):844–51. Available from:
518 <http://www.ncbi.nlm.nih.gov/pubmed/9812080>
- 519 17. Zheng X, Walcott GP, Hall JA, Rollins DL, Smith WM, Kay GN, et al. Electrode
520 impedance: an indicator of electrode-tissue contact and lesion dimensions during linear
521 ablation. *J Interv Card Electrophysiol* [Internet]. 2000 Dec [cited 2015 Nov
522 11];4(4):645–54. Available from: <http://www.ncbi.nlm.nih.gov/pubmed/11141212>
- 523 18. Gunawardene M, Münkler P, Eickholt C, Akbulak RÖ, Jularic M, Klatt N, et al. A
524 novel assessment of local impedance during catheter ablation: initial experience in
525 humans comparing local and generator measurements. *EP Eur* [Internet]. 2019 Jan 1
526 [cited 2019 Oct 4];21(Supplement_1):i34–42. Available from:
527 <http://www.ncbi.nlm.nih.gov/pubmed/30801126>
- 528 19. Gallagher NP, Fear EC, Vigmond EJ, Byrd IA. Catheter contact geometry affects
529 lesion formation in radio-frequency cardiac catheter ablation. *Conf Proc . Annu Int*
530 *Conf IEEE Eng Med Biol Soc IEEE Eng Med Biol Soc Annu Conf* [Internet]. 2011
531 Aug [cited 2019 Oct 4];2011:243–6. Available from:
532 <http://ieeexplore.ieee.org/document/6090046/>
- 533 20. Rolf S, Boldt L-H, Parwani AS, Wutzler A, Huemer M, Blaschke D, et al. Findings
534 and outcome of fluoroscopic visualization of the oesophageal course during catheter
535 ablation of atrial fibrillation. *Europace* [Internet]. 2011 Jun 1 [cited 2019 Oct
536 4];13(6):796–802. Available from: <http://www.ncbi.nlm.nih.gov/pubmed/21398313>

- 537 21. Mohanty S, Santangeli P, Mohanty P, Biase L Di, Trivedi C, Bai R, et al. Outcomes of
538 atrioesophageal fistula following catheter ablation of atrial fibrillation treated with
539 surgical repair versus esophageal stenting. *J Cardiovasc Electrophysiol* [Internet]. 2014
540 Jun [cited 2017 Nov 20];25(6):579–84. Available from:
541 <http://www.ncbi.nlm.nih.gov/pubmed/25013875>
- 542 22. Avitall B, Mughal K, Hare J, Helms R, Krum D. The effects of electrode-tissue contact
543 on radiofrequency lesion generation. *Pacing Clin Electrophysiol* [Internet]. 1997 Dec
544 [cited 2019 Oct 4];20(12 Pt 1):2899–910. Available from:
545 <http://doi.wiley.com/10.1111/j.1540-8159.1997.tb05458.x>
- 546 23. Bortone A, Appetiti A, Bouzeman A, Maupas E, Ciobotaru V, Boulenc J-M, et al.
547 Unipolar signal modification as a guide for lesion creation during radiofrequency
548 application in the left atrium: prospective study in humans in the setting of paroxysmal
549 atrial fibrillation catheter ablation. *Circ Arrhythm Electrophysiol* [Internet]. 2013 Dec
550 [cited 2015 Nov 11];6(6):1095–102. Available from:
551 <http://www.ncbi.nlm.nih.gov/pubmed/24097371>
- 552 24. Pambrun T, Durand C, Constantin M, Masse A, Marra C, Meillet V, et al. High-Power
553 (40–50 W) Radiofrequency Ablation Guided by Unipolar Signal Modification for
554 Pulmonary Vein Isolation. *Circ Arrhythmia Electrophysiol* [Internet]. 2019 Jun [cited
555 2019 Oct 4];12(6):e007304. Available from:
556 <http://www.ncbi.nlm.nih.gov/pubmed/31164003>
- 557 25. Baher A, Kheirkhahan M, Rechenmacher SJ, Marashly Q, Kholmovski EG,
558 Siebermair J, et al. High-Power Radiofrequency Catheter Ablation of Atrial
559 Fibrillation. *JACC Clin Electrophysiol* [Internet]. 2018 Dec [cited 2019 Jan
560 23];4(12):1583–94. Available from: <http://www.ncbi.nlm.nih.gov/pubmed/30573123>

- 561 26. Reddy VY, Grimaldi M, De Potter T, Vijgen JM, Bulava A, Duytschaever MF, et al.
562 Pulmonary Vein Isolation With Very High Power, Short Duration, Temperature-
563 Controlled Lesions. *JACC Clin Electrophysiol* [Internet]. 2019 Jul [cited 2019 Oct
564 4];5(7):778–86. Available from: <http://www.ncbi.nlm.nih.gov/pubmed/31320006>
- 565 27. Irastorza RM, d'Avila A, Berjano E. Thermal latency adds to lesion depth after
566 application of high-power short-duration radiofrequency energy: Results of a
567 computer-modeling study. *J Cardiovasc Electrophysiol* [Internet]. 2018 Feb [cited
568 2019 Jan 23];29(2):322–7. Available from:
569 <http://www.ncbi.nlm.nih.gov/pubmed/28988468>
- 570 28. Nakagawa H, Wittkamp FH, Yamanashi WS, Pitha J V, Imai S, Campbell B, et al.
571 Inverse relationship between electrode size and lesion size during radiofrequency
572 ablation with active electrode cooling. *Circulation* [Internet]. 1998 Aug 4 [cited 2019
573 Oct 4];98(5):458–65. Available from: <http://www.ncbi.nlm.nih.gov/pubmed/9714097>
- 574 29. Bourier F, Schwarz B, Brkic A, Wolff L, Semmler V, Kottmaier M, et al. EP
575 radiofrequency generators: Significant offsets between selected and delivered power? *J*
576 *Cardiovasc Electrophysiol* [Internet]. 2018 Feb [cited 2019 Oct 4];29(2):330–4.
577 Available from: <http://www.ncbi.nlm.nih.gov/pubmed/29149500>
- 578
- 579
- 580
- 581
- 582